Science of the Total Environment 858 (2023) 160064

Contents lists available at ScienceDirect

Science of the Total Environment

journal homepage: www.elsevier.com/locate/scitotenv

Review

Trends in urban air pollution over the last two decades: A global perspective

Pierre Sicard [a,*], Evgenios Agathokleous [b], Susan C. Anenberg [c], Alessandra De Marco [d], Elena Paoletti [e], Vicent Calatayud [f]

[a] ARGANS, 260 route du Pin Montard, Biot, France
[b] School of Applied Meteorology, NUIST, Nanjing, China
[c] George Washington University, Milken Institute School of Public Health, United States
[d] ENEA, C.R., Casaccia, Italy
[e] IRET-CNR, Sesto Fiorentino, Italy
[f] Fundación CEAM, Parque Tecnológico, C/Charles R. Darwin, 14, Paterna, Spain

HIGHLIGHTS

- We used 20-year of observationally constrained modelled data and ground-based observations covering 13,160 urban areas.
- We estimated the city-level trends of urban population exposure to O_3, $PM_{2.5}$, and NO_2.
- Global PM2.5 exposure declined (− 0.2 % year^{-1}) with 65 % of cities showing rising levels.
- The annual NO_2 mean concentrations increased at 71 % of cities (+ 0.4 % year^{-1}).
- Global exposure of urban population to O_3 increased at 89 % of stations (+ 0.8 % year^{-1}).

GRAPHICAL ABSTRACT

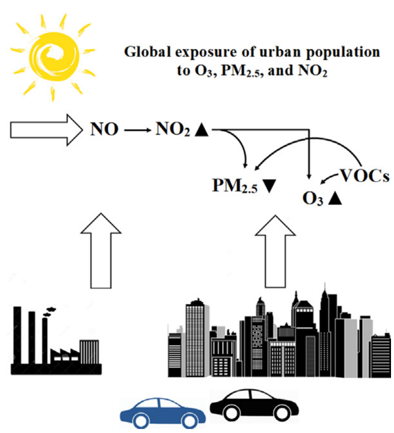

ARTICLE INFO

Editor: Philip K. Hopke

Keywords:
Air pollution trends
Human health
Population exposure
Urban areas
Global burden of diseases
Risk assessment

ABSTRACT

Ground-level ozone (O_3), fine particles ($PM_{2.5}$), and nitrogen dioxide (NO_2) are the most harmful urban air pollutants regarding human health effects. Here, we aimed at assessing trends in concurrent exposure of global urban population to O_3, $PM_{2.5}$, and NO_2 between 2000 and 2019. $PM_{2.5}$, NO_2, and O_3 mean concentrations and summertime mean of the daily maximum 8-h values (O_3 MDA8) were analyzed (Mann-Kendall test) using data from a global reanalysis, covering 13,160 urban areas, and a ground-based monitoring network (Tropospheric Ozone Assessment Report), collating surface O_3 observations at nearly 10,000 stations worldwide. At global scale, $PM_{2.5}$ exposures declined slightly from 2000 to 2019 (on average, − 0.2 % year^{-1}), with 65 % of cities showing rising levels. Improvements were observed in the Eastern US, Europe, Southeast China, and Japan, while the Middle East, sub-Saharan Africa, and South Asia experienced increases. The annual NO_2 mean concentrations increased globally at 71 % of cities (on average, +0.4 % year^{-1}), with improvements in North America and Europe, and increases in exposures in sub-Saharan Africa, Middle East, and South Asia regions, in line with socioeconomic development. Global exposure of urban population to O_3 increased (on average, +0.8 % year^{-1} at 89 % of stations), due to lower O_3 titration by NO. The summertime O_3 MDA8 rose at 74 % of cities worldwide (on average, +0.6 % year^{-1}), while a decline was observed in North America, Northern Europe, and Southeast China, due to the reduction in precursor emissions. The highest O_3 MDA8 increases (>3 % year^{-1}) occurred in Equatorial Africa, South Korea, and India. To reach air quality standards and

* Corresponding author.
E-mail address: psicard@argans.eu (P. Sicard).

http://dx.doi.org/10.1016/j.scitotenv.2022.160064
Received 20 July 2022; Received in revised form 3 November 2022; Accepted 4 November 2022
Available online 8 November 2022
0048-9697/© 2022 Elsevier B.V. All rights reserved.

mitigate outdoor air pollution effects, actions are urgently needed at all governance levels. More air quality monitors should be installed in cities, particularly in Africa, for improving risk and exposure assessments, concurrently with implementation of effective emission control policies that will consider regional socioeconomic imbalances.

Contents

1. Introduction

Outdoor air pollution is a major global public health issue (Cohen et al., 2017), leading to 4.14 million non-accidental premature deaths in both urban and rural areas worldwide in 2019 alone (Global Burden of Disease, 2019). In 2016, 54 % of the world's population lived in urban areas (United Nations, 2018), where ground-level ozone (O_3), particles with an aerodynamic diameter lower than 2.5 μm ($PM_{2.5}$), and nitrogen dioxide (NO_2) are the most harmful air pollutants for human health (Pascal et al., 2013; McDuffie et al., 2021; Anenberg et al., 2022). By 2050, 70 % of the world's population will reside urban areas (United Nations, 2018), and outdoor air pollution would lead to about 6.6 million premature deaths (Lelieveld et al., 2015). Air pollution also adversely affects biodiversity, ecosystems, and ecosystem services, such as nutrient cycling (Agathokleous et al., 2020; Hu et al., 2022; Perring et al., 2022).

Since the 1990s, anthropogenic air pollutants emissions (nitrogen oxides NO_x, Volatile Organic Compounds VOCs, and PM) have decreased in North America and Europe (Shaddick et al., 2020; Sicard et al., 2020a; Zara et al., 2021) but increased in East Asia (Lin et al., 2017; Zheng et al., 2018), India (Itahashi et al., 2019), and Middle East (Barkley et al., 2017). In China, NO_x emissions peaked around 2011, and subsequently declined (Liu et al., 2017; Zheng et al., 2018). However, even in the cases where emissions decreased, the exposures remain elevated enough to pose risks to human health (e.g., Health Effects Institute, 2020; European Environment Agency, 2021; Khomenko et al., 2021). In 2019, billions of people were exposed to concentrations of $PM_{2.5}$ (Southerland et al., 2022), O_3 (Sicard, 2021), and NO_2 (Anenberg et al., 2022) above the World Health Organization (WHO) Air Quality Guidelines 2005 (AQG) for human health protection. For instance, 74 %, 4 %, and 99 % of the European urban population was exposed to $PM_{2.5}$ (10 μg m^{-3}), NO_2 (40 μg m^{-3}), and O_3 (8h daily max <50 ppb) levels above the WHO's 2005 limit values, respectively (European Environment Agency, 2021). These percentages would be even higher if the new WHO AQG introduced in 2021 [$PM_{2.5}$ (5 μg m^{-3}), NO_2 (10 μg m^{-3}), and O_3 (peak season <30 ppb)] are considered in future evaluations.

In 2019, the urban population exposure exceeding the annual WHO's 2005 limit value for $PM_{2.5}$ (10 μg m^{-3}) led to 1.8 million attributable deaths in 13,160 urban areas with >50,000 inhabitants (Southerland et al., 2022). Similarly, the chronic O_3 exposure led to 147,100 deaths in such cities in 2019 (Malashock et al., 2022). The NO_x, as key precursors, cause $PM_{2.5}$- and O_3-related premature deaths globally (Anenberg et al., 2017). Anenberg et al. (2022) have limited the NO_2 analyses to pediatric asthma incidence, to avoid potential overlap with $PM_{2.5}$, and have estimated that 1.85 million pediatric asthma cases were attributable to NO_2 in 13,189 cities in 2019 globally.

Following the establishment of air quality standards and emission control policies (e.g., MEP - Ministry of Environmental Protection, 2012; European Council Directive 2008/50/EC, 2008; United States Federal Register, 2015; European Council Directive 2016/2284/EC, 2016), the number of air quality monitoring stations increased rapidly worldwide. The Tropospheric Ozone Assessment Report (TOAR), initiated by the International Global Atmospheric Chemistry Project, gathers surface O_3 measurements from monitoring stations worldwide (Schultz et al., 2017). However, the spatial distribution of monitoring stations tends to be heterogeneous, and gaps within time series can be noted for suitable human health and ecological risk assessments (Araki et al., 2015; De Marco et al., 2022). For example, ground $PM_{2.5}$ measurements are missing for sites representing >50 % of the world's urban population (Apte et al., 2021). To overcome this issue and characterize air pollutants concentrations, particularly for regions where monitoring data are sparse, the Global Reanalysis Datasets (GRD) combine satellite observations, chemical transport models, and data from ground-based monitoring networks to improve model predictions and estimates of population exposure (Hammer et al., 2020; Anenberg et al., 2022; Southerland et al., 2022).

The Global Burden of Diseases (GBD) is a collaborative research initiative assessing mortality due to 369 diseases and injuries, and 87 risk factors, including air pollution in 204 countries and territories (Global Burden of Disease, 2019). Estimates for population exposure to $PM_{2.5}$ and O_3 in 13,160 urban areas with over 50,000 inhabitants were obtained from the Global Burden of Disease (2019), while the NO_2 concentration dataset were provided by Anenberg et al. (2022). Anenberg et al. (2022), Malashock et al. (2022), and Southerland et al. (2022) have provided urban average concentrations of the surface-level annual $PM_{2.5}$ and NO_2 mean concentrations and the highest seasonal (summertime, e.g., April–September at 45°N latitude) average daily 8-h maximum O_3 concentration (abbreviated as "summertime O_3 MDA8") for all cities worldwide at a fine spatial resolution from 2000 to 2019 (GRD).

Due to the length of time series and spatial coverage, both the TOAR database and GRD offer an unprecedented opportunity to simultaneously analyze trends in surface $PM_{2.5}$, O_3, and NO_2 metrics. Previous papers did not provide a deep trend analysis per country, which is profoundly important to tackle inequalities among countries with respect to the agenda of the United Nations (UN) Sustainable Development Goals (SDGs). Hence, we conducted a 20-year assessment aiming at: i) detecting and estimating the annual city-level trends in $PM_{2.5}$ and NO_2 mean concentrations and human health-related O_3 metric from 2000 to 2019 in urban areas using robust statistical testing; ii) assessing the impacts of emissions control policies on exposure of urban population to outdoor air pollution; and iii) comparing for the first time O_3 MDA8 trends obtained from ground-based monitoring networks (TOAR) and modeling (GRD). For the first time, we provide both observation-based and model-based trends with a concrete estimation of the magnitude per country at global scale. In this study, we hypothesized that short-term changes over 20-year time-series are attributed to emissions changes. To capture any changes over time, we have calculated the trend magnitude over the time periods 2000–2009 and 2010–2019, in addition to 2000–2019 for all countries.

2. Materials and methods

2.1. Ground measurements

The TOAR database (https://join.fz-juelich.de) gathers surface O_3 observations from 10,030 monitoring stations around the world since the 1970s (Schultz et al., 2017). For the robustness of the study, we applied criteria in selecting stations. We selected monitoring stations with >50,000 inhabitants in a radius of 5 km around the station location and with over 75 % of validated hourly data per year, for a minimum time period of 10 years from 2000 onward. In China, the surface O_3 monitoring started in 2013, thus the Chinese stations were not included for ground measurements analyses. Finally, 519 urban monitoring stations were selected from 28 countries worldwide over the time period 2000–2019. From year to year, the number of monitoring stations did not significantly change.

In previous epidemiological studies, the summertime O_3 MDA8 was significantly correlated with all-causes, respiratory, and circulatory mortalities (Bell et al., 2007; Jerrett et al., 2009; Turner et al., 2016; Lefohn et al., 2018). In our study, we investigated: i) the annual O_3 mean concentrations incorporating both high and low O_3 exposures, and ii) the summertime O_3 MDA8 to represent the higher O_3 exposure levels of population in urban areas (Lefohn et al., 2018).

2.2. Global Reanalysis Dataset (GRD)

The urban built-up area is from the Global Human Settlement Layer - Settlement Model (GHS-SMOD dataset[1]) to categorize all grid cells as urban area, and the high-resolution geospatial data on population distribution is from the Worldpop dataset[2] at about 1 km of spatial resolution for all years from 2000 to 2019 (Tatem, 2017; Lloyd et al., 2019). Finally, 13,160 urban areas (from 176 countries) were defined with >50,000 inhabitants. In all grid cells categorized as urban according to the GHS-SMOD, estimates for $PM_{2.5}$, NO_2, and O_3 levels were obtained.

In short, the surface annual $PM_{2.5}$ mean concentrations were obtained from Hammer et al. (2020) at high spatial resolution (about 1 km × 1 km at the equator), and recently used by Southerland et al. (2022). The $PM_{2.5}$ dataset includes satellite-retrieved aerosol optical depth from three satellite sensors (Moderate Resolution Imaging Spectroradiometer, Sea-viewing Wide Field-of-View Sensor, and the Multiangle Imaging Spectroradiometer), the global 3-D chemical GEOS-Chem model (Goddard Earth Observing System), combined to ground-based observations of $PM_{2.5}$ (>10,400 monitoring stations from 116 countries) using a geographically weighted regression (Hammer et al., 2020; Southerland et al., 2022). The estimated annual mean $PM_{2.5}$ concentrations are well correlated (coefficient of determination $r^2 = 0.90$–0.92) to ground-based measurements (Southerland et al., 2022).

The dataset of annual NO_2 mean concentrations (1 km × 1 km spatial resolution) was developed by Larkin et al. (2017) and Anenberg et al. (2022), by combining annual measurements from a land use regression model from 5220 air monitors in 58 countries (mostly in Asia, Europe, and North America) with tropospheric NO_2 column observations and reanalysis from O_3 Monitoring Instrument satellite (Larkin et al., 2017). The estimated annual mean NO_2 concentrations are well correlated to ground-based measurements with r^2 ranged from 0.42 in Africa to 0.67 in South America, and $r^2 = 0.52$–0.54 in North America, Europe, and Asia (Larkin et al., 2017).

Most of epidemiological studies used summertime O_3 MDA8 as human health-related O_3 metric (Global Burden of Disease, 2019). De Lang et al. (2021) used M3Fusion and Bayesian Maximum Entropy Data Fusion to integrate ground-level O_3 measurements from the TOAR and the Chinese National Environmental Monitoring Center Network (8834 monitoring sites globally) with nine global atmospheric chemistry models based on their ability to predict observations in each region and year. The summertime O_3 MDA8 was calculated as the annual maximum of the six-month running mean of the average daily 8-h maximum O_3 concentration. The summertime O_3 MDA8 were produced across the entire globe for every year from 2000 to 2019 at a spatial resolution of approximately 11 km at the equator. For our analyses, we used regridded O_3 data from 11 km to 1 km resolution (Malashock et al., 2022). By ground validation, the approach led to greater confidence in the model predictions ($r^2 = 0.81$ at the test point, and $r^2 = 0.63$ at 0.1° of resolution) and estimates of human exposures (De Lang et al., 2021). The O_3 MDA8 dataset was recently used by Malashock et al. (2022) for all cities worldwide.

2.3. Statistical estimation of annual trends

To assess short-term changes, a 20-year time-series is long enough (Monks et al., 2015) as the observed changes are likely attributed to emissions changes rather than meteorological variations (Sicard, 2021). Both non-parametric Mann-Kendall test and Sen's slope estimator were applied to detect and estimate the trend magnitude within time-series (Sicard et al., 2016). Both tests were applied for the modelled annual $PM_{2.5}$ and NO_2 mean concentrations and summertime O_3 MDA8 (GRD dataset) in 13,160 urban areas (in 176 countries including China) with >50,000 inhabitants over the time period 2000–2019. Both tests were also applied for the observed annual O_3 mean concentrations and summertime O_3 MDA8 (TOAR dataset) in 519 urban monitoring stations (with >50,000 inhabitants in a radius of 5 km excluding China). For all countries, we have calculated the trend magnitude over three time periods, 2000–2009, 2010–2019, and 2000–2019, in order to capture changes over time. Results were considered statistically significant at a p value of <0.05. For each country, a country-averaged urban trend magnitude was calculated from

[1] https://ghsl.jrc.ec.europa.eu/ghs_smod2019.php

[2] https://www.worldpop.org/

trends at $p < 0.05$ (in % per year) as well as the percentage of urban areas with an increase/decrease trend. The 1-km resolution of data is not important here as we analyzed trends magnitude over time, thus we captured well the trends for a given location.

For the first time, we compared the 20-year O_3 MDA8 trends calculated from the GRD (simulated) with the trends calculated from the TOAR database (observed). For that, we computed pointwise the Root Mean Square Error (RMSE) and the Mean Bias (MB) between the simulated and measured values, and then averaged for each country. The RMSE provides information about the short-term performance of a model by allowing a term-by-term comparison of the actual difference between the estimated and the measured value. The MB provides the absolute bias of the model, with negative and positive values indicating underestimation and overestimation by the model.

3. Results

3.1. Trends in $PM_{2.5}$ concentrations in urban areas

For annual $PM_{2.5}$ mean concentrations, 65 % of the urban areas showed an increase between 2000 and 2019 (Table 1S). The trends magnitude

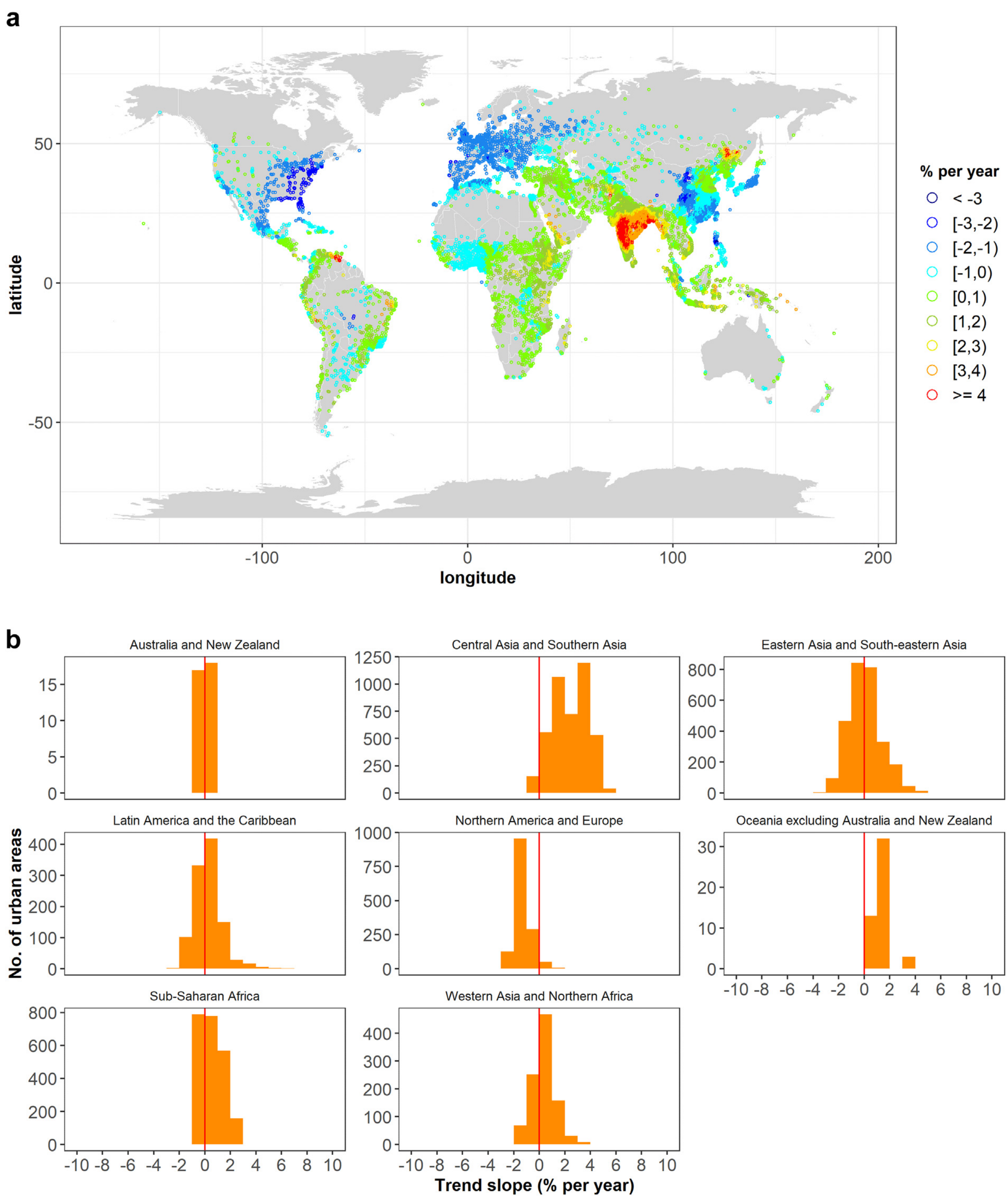

Fig. 1. a: Annual trends in $PM_{2.5}$ mean concentrations (in % per year) in urban areas with >50,000 inhabitants over the time period 2000–2019.
b: Frequency distribution of the trends of $PM_{2.5}$ annual mean concentrations (in % per year) in urban areas with >50,000 inhabitants over the time period 2000–2019.

varied widely among regions (Fig. 1a). From 2000 to 2019, >2 % year^{-1} reductions in $PM_{2.5}$ were observed in the Eastern US, 1–2 % year^{-1} reductions in North America, Europe, Western Africa, and Eastern Asia, 1–2 % year^{-1} increases in Southeast Asia, the Middle East, parts of South America and East Africa, and >3 % year^{-1} increases in South Asia (Fig. 1b). There is a small area of positive trends over Eastern China, e.g., in Heilongjiang region (> 3 % per year). From 2000 to 2019, the average annual $PM_{2.5}$ mean concentrations increase was 3.1 % year^{-1} in all urban areas in Bangladesh, and 2.8 % year^{-1} at 99 % of Indian urban areas (Table 1S). Between 2000 and 2019, the annual $PM_{2.5}$ mean concentrations decreased by 1.2 % year^{-1} in Canada, with 85 % of urban areas showing a decline, and declined by 1.5 % year^{-1} in 95 % of the US urban areas and by 1.2 % year^{-1} at 99 % of EU-28 urban centers (Table 1S).

By comparing the time periods 2000–2009 (Fig. 1S) and 2010–2019 (Fig. 2S), the main changes were observed in the Middle East and Asia, with sustained $PM_{2.5}$ increases in South Asian urban areas conversely to improvements in Chinese urban areas. At global scale, the annual averaged $PM_{2.5}$ concentrations increased in 59 % of urban areas between 2000 and 2009 (Table 2S), and in 45 % of urban areas between 2010 and 2019 (Table 3S). Between 2000 and 2009, the annual $PM_{2.5}$ levels declined by 2.1 % year^{-1} in Canada, by 1.9 % year^{-1} in the US, and by 1.7 % year^{-1} in EU-28 urban centers, where 98 %, 88 %, and 95 % of urban areas exhibited a decrease, respectively. These figures are lower over the time period 2010–2019: - 0.1 % year^{-1} in Canada, − 1.2 % year^{-1} in the US, and - 1.8 % year^{-1} in EU-28, with respectively 74 %, 78 %, and 91 % of urban areas showing a decrease. An increase in $PM_{2.5}$ was observed at 78 % of China's urban areas (on average + 1.6 % year^{-1}) over the period 2000–2009, whereas 97 % of Chinese urban areas exhibited a decrease (on av. - 3.5 % year^{-1}) between 2010 and 2019. In India, the trends were quite similar to China over both decades, i.e., on average + 1.6 % year^{-1} with 85 % of urban areas showing an increase in $PM_{2.5}$ in 2000–2009, and + 1.2 % year^{-1} with 78 % of urban areas showing a decrease in 2010–2019.

3.2. Trends in NO_2 concentrations in urban areas

At global scale, the annual averaged NO_2 concentrations increased at 71 % of the urban areas between 2000 and 2019 (Table 1S). From 2000 to 2019, >2 % year^{-1} reductions in NO_2 were observed in the North America and Western Europe, 1–2 % year^{-1} reductions in central Europe, equatorial Africa, and parts of Eastern Asia, while 1–2 % year^{-1} increases were observed in South America, Africa, Middle East, and South Asia. In South Asia, higher than 4 % year^{-1} increases were reported (Fig. 2. a). Except in the US and Europe, the spatial distribution of trend magnitude is widely heterogeneous (Fig. 2. a). From 2000 to 2019, the annual averaged NO_2 concentrations increased by 2.4 % year^{-1} in all urban areas in Bangladesh, by 3.2 % year^{-1} in 92 % of urban areas in Vietnam, and by 2.2 % year^{-1} at 99 % of Indian urban areas (Table 1S). In the Middle East, the NO_2 levels increased by 1.6 % per year at 90 % of urban areas over the time period 2000–2019. In China, 56 % of urban areas showed an increase in NO_2 levels with an averaged trend of +0.5 % per year. The annual averaged NO_2 concentrations decreased by 2.1 % year^{-1} in 96 % of urban areas in Canada, by 2.8 % year^{-1} in all urban areas in the US, and by 1.1 % year^{-1} at 95 % of EU-28 urban areas (Table 1S).

By comparing both time periods 2000–2009 (Fig. 3S) and 2010–2019 (Fig. 4S), the main changes were observed in central (e.g., Poland) and Southwestern Europe (Portugal, Spain), the Middle East and Eastern Asia, with strong improvements in Chinese urban areas. At global scale, the annual averaged NO_2 concentrations increased in 69 % of urban areas between 2000 and 2009 (Table 2S) and in 55 % of urban areas between 2010 and 2019 (Table 3S). In China, surface NO_2 increased at 85 % of urban areas (on av. + 1.6 % year^{-1}) over the period 2000–2009, while 93 % of Chinese urban areas reported a decrease (on av. - 3.5 % year^{-1}) between 2010 and 2019. In the Middle East, the NO_2 levels increased by 3.1 % year^{-1} over 2000–2009 and by 1.8 % year^{-1} over 2010–2019. In the EU-28 countries, the annual averaged NO_2 concentrations slightly increased by 0.1 % year^{-1}, while 77 % of urban areas showed a decrease over the time period 2000–2009. The NO_2 levels also declined by 1.1 % year^{-1}, with 87 % of urban areas showing a decrease between 2010 and 2019. In Portugal and Spain, the surface NO_2 concentrations increased by 4.6–4.7 % year^{-1} between 2000 and 2009 (in >85 % of urban centers) and declined by 1.6–2.8 % year^{-1} from 2010 to 2019 in >90 % of urban areas (Table 2S—3S). In all urban areas in Poland, NO_2 decreased (− 1.0 % year^{-1}) from 2000 to 2009, with a further decrease (− 3.5 % year^{-1}) from 2010 to 2019. Between 2000 and 2009, the annual NO_2 levels declined by 2.9 % year^{-1} in Canada and by 2.6 % year^{-1} in the US, with 96 % and 98 % of urban areas exhibiting a decrease, respectively. From 2010 to 2019, we found - 0.8 % year^{-1} in Canada, and - 2.2 % year^{-1} in the US with 74 %, and 93 % of urban areas showing a decrease.

3.3. Trends in urban population exposure to O_3

3.3.1. Simulated versus observed trends in summertime O_3 MDA8

The RMSE between the simulated (GRD) and measured (TOAR) values for the whole domain was 1.026 ppb year^{-1} (data not shown). For the whole domain, the averaged MB was 0.11 ppb year^{-1} (overestimation). The largest discrepancies (overestimation) were observed in Mexico (+ 1.59 ppb year^{-1}), The Netherlands (+ 0.97 ppb year^{-1}), and Taiwan (+ 0.83 ppb year^{-1}) while the best performance with slight underestimations were observed in Germany (− 0.04 ppb year^{-1}), Israel (− 0.05 ppb year^{-1}), and Spain (− 0.07 ppb year^{-1}).

3.3.2. Trends in summertime O_3 MDA8

The summertime O_3 MDA8, calculated from the GRD, increased at 74 % of the urban areas between 2000 and 2019 (Table 1S). From 2000 to 2019, reductions in summertime O_3 MDA8 occurred in the North and Central America, Northern Europe, Japan, and Southeastern China. Conversely, we observed increases of 1–2 % year^{-1} in South America, North Africa, sub-Saharan and South Africa, Middle East, Northeastern China, and South Asia, and higher increases (>3 % year^{-1}) in Equatorial Africa, South Korea, and India (Fig. 3a-b). From 2000 to 2019, the trends in summertime O_3 MDA8 ranged between −1 and + 1 % year^{-1} in Central and Southern Europe. The summertime O_3 MDA8 decreased by on average 0.7 % year^{-1} in the US, with 88 % of urban areas showing an O_3 MDA8 decrease; 0.5 % year^{-1} in 92 % of urban areas in Northern Europe and 0.2 % year^{-1} in China in 67 % of urban areas (Table 1S). In Southern and Central Europe, the averaged trend was 0.1 % year^{-1}. In Northern Africa, the summertime O_3 MDA8 increased by 0.6 % year^{-1} at 87 % of urban areas, while an increase of 2.3 % year^{-1} was noted in 96 % of urban areas in Democratic Republic of the Congo. The increase trend was 1.3 % year^{-1} in all Indian urban areas, and 2.5 % year^{-1} in all South Korean urban areas. Also, an increase trend of 2.1, 3.8, and 4.2 % year^{-1} was observed in all urban areas of Ethiopia, Somalia, and the Republic of the Congo, respectively, over the time period 2000–2019 (Table 1S).

Considering both time periods, 2000–2009 (Fig. 5S) and 2010–2019 (Fig. 6S), strong improvements were observed in East Asia, while O_3 MDA8 increases were found in India and in some parts of South America e.g., Peru and Brazil in particular nearby Sao Paulo. At global scale, the summertime O_3 MDA8 increased in 85 % of urban areas between 2000 and 2009 (Table 2S) and in 72 % of urban areas between 2010 and 2019 (Table 3S). In East Asia, summertime O_3 MDA8 increased in 99 % of urban areas in China (on average + 2.0 % year^{-1}) and in 79 % of urban areas in Japan (on average + 1.0 % year^{-1}) over the period 2000–2009. Conversely, O_3 MDA8 significantly decreased in 76 % of Chinese urban areas (on average - 1.0 % year^{-1}) and in 80 % of urban areas in Japan (on average - 0.7 % year^{-1}) between 2010 and 2019. In India, the O_3 MDA8 increased by 0.9 % per year in 2000–2009 and by 2.0 % per year in 2010–2019 in all urban areas. In Brazil, the O_3 MDA8 decreased by 0.1 % year^{-1} between 2000 and 2009 (in 59 % of urban centers) and increased by 1.7 % year^{-1} from 2010 to 2019 in 99 % of urban areas. In the EU-28 countries, the summertime O_3 MDA8 slightly increased by on average 0.1 % year^{-1}, with 60 % of urban areas showing an O_3 MDA8

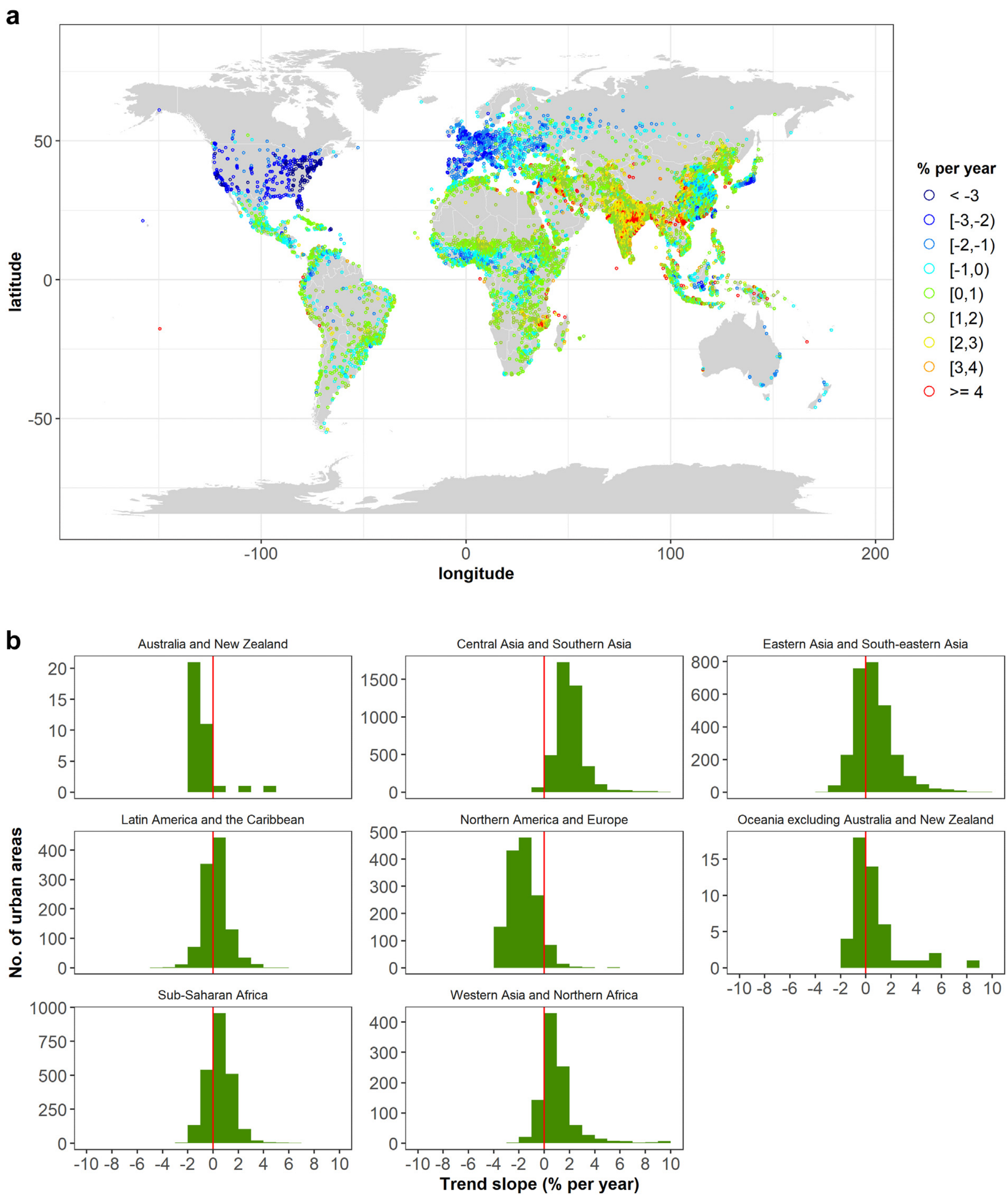

Fig. 2. a: Annual trends in NO2 mean concentrations (in % per year) in urban areas with >50,000 inhabitants over the time period 2000–2019.
b: Frequency distribution of the trends of NO_2 annual mean concentrations (in % per year) in urban areas with >50,000 inhabitants over the time period 2000–2019. Outliers over 10 % not represented for the sake of clarity.

increase between 2000 and 2009 (Table 2S), and declined by 0.3 % $year^{-1}$, while 61 % of urban areas showed an increase between 2010 and 2019 (Table 3S). In the US, the O_3 MDA8 decreased by 0.6 % $year^{-1}$ between 2000 and 2009 (in 87 % of urban centers) and by 0.9 % $year^{-1}$ from 2010 to 2019 in 84 % of urban areas. In Canada, the trend is quite null (− 0.04 % $year^{-1}$) between 2000 and 2009, while O_3 MDA8 declined by 0.9 % $year^{-1}$ at 80 % of urban areas between 2010 and 2019.

From ground measurements stations (included in TOAR database), the summertime O_3 MDA8 decreased by on average 0.5 % $year^{-1}$, with 71 % of EU cities showing a O_3 MDA8 decrease between 2000 and 2019 (Fig. 4, Table 4S). The highest decreases were observed in the Netherlands (on average - 1.3 % $year^{-1}$) and Ireland (on average - 1.8 % $year^{-1}$), while the highest increases were recorded in Spain (on average + 0.4 % $year^{-1}$) and Bulgaria (on average + 0.9 % $year^{-1}$). In Canada and the US, the summertime O_3 MDA8 significantly decreased by about 0.8 % $year^{-1}$, with 67 % and 92 % of cities, respectively, showing a decrease between 2000 and 2019 (Fig. 4). In Brazil, the summertime O_3 MDA8 increased by 0.4 % per year. In East Asia,

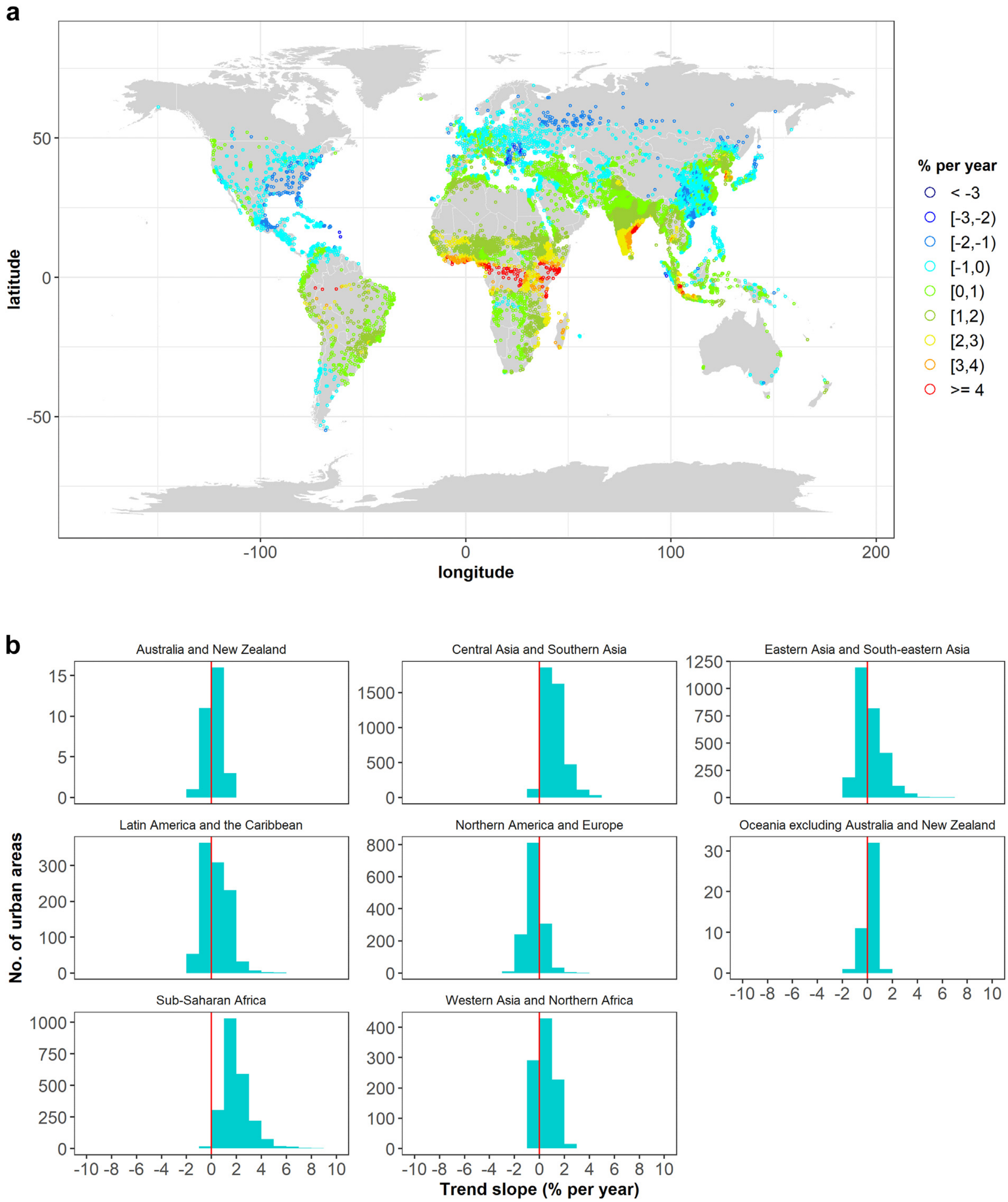

Fig. 3. a: Annual trends in the highest seasonal average daily 8-h maximum O_3 concentration (in % per year) in urban areas with >50,000 inhabitants, from the global reanalysis datasets, over the time period 2000–2019.
b: Frequency distribution of the trends of the highest seasonal average daily 8-h maximum O_3 concentration (in % per year) in urban areas with >50,000 inhabitants over the time period 2000–2019.

the summertime O_3 MDA8 increased in 92 % of cities in South Korea (on average + 1.9 % $year^{-1}$) and decreased in 76 % of cities in Japan (on average - 0.6 % $year^{-1}$) between 2010 and 2019 (Table 4S).

3.3.3. Trends in annual O_3 mean concentrations

A rise was observed in 84 % of the 154 urban centers in the EU (on average + 0.5 % $year^{-1}$) between 2000 and 2019 (Fig. 5, Table 4S). In the EU, a decline of O_3 levels was observed in Ireland (on average - 1.7 % $year^{-1}$), Hungary (on average - 0.6 % $year^{-1}$), and Poland (on average - 0.4 % $year^{-1}$), whereas the highest increases were recorded in Bulgaria (on average + 2.2 % $year^{-1}$) and Spain (on average + 2.4 % $year^{-1}$). In Canada and the US, the annual O_3 mean concentrations increased by 2.4 % $year^{-1}$ and 1.6 % $year^{-1}$, with 100 % and 90 % of urban areas, respectively, showing rising O_3 levels between 2000 and 2019. In East

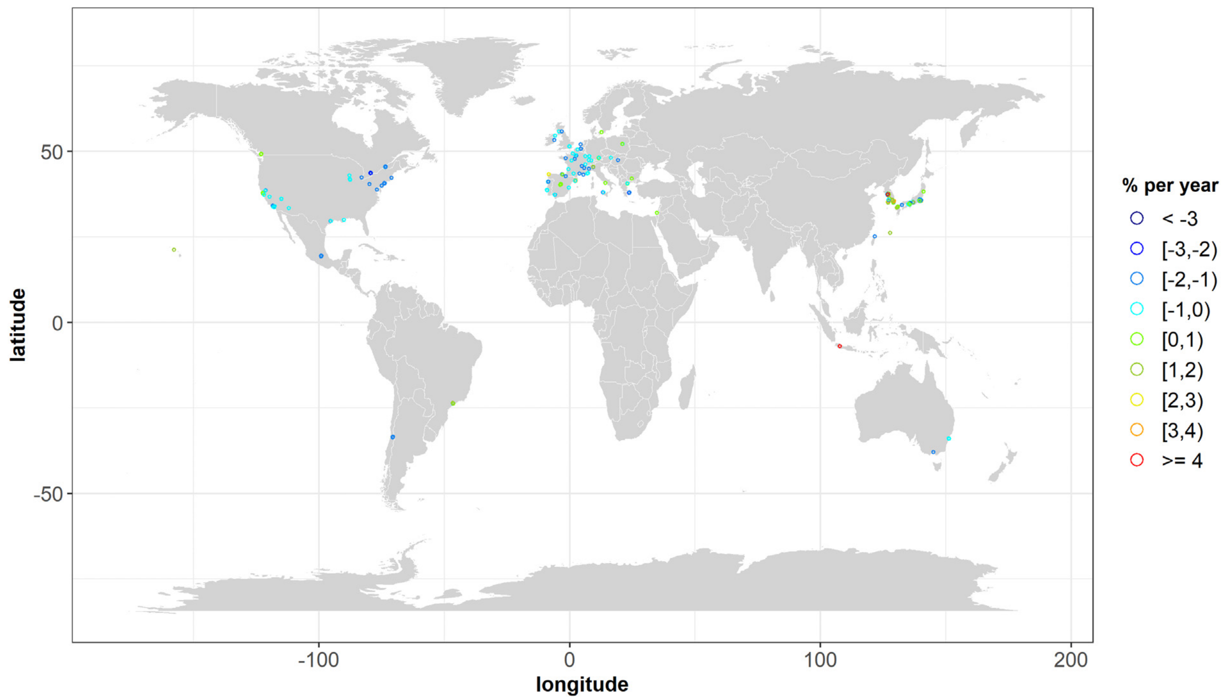

Fig. 4. Annual trends in the highest seasonal average daily 8-h maximum O_3 concentration (in % per year) in urban areas with >50,000 inhabitants, from ground-based monitoring networks (Tropospheric Ozone Assessment Report) over the time period 2000–2019.

Asia, rising O_3 levels are observed in 98 % of urban areas in South Korea (on average + 3.9 % $year^{-1}$) and in 91 % of urban areas in Japan (on average + 1.4 % $year^{-1}$) between 2010 and 2019 (Table 4S). In Australia, the urban O_3 levels rose by 1.1 % $year^{-1}$. In America, Chile (on average - 1.0 % $year^{-1}$) and Mexico (on average - 1.3 % $year^{-1}$) showed a decline of O_3 levels in urban areas.

4. Discussion

4.1. Trends in $PM_{2.5}$ concentrations in urban areas

The highest annual $PM_{2.5}$ mean concentrations were observed in East and South Asia (>45 μg m^{-3}), in particular in India (>75 μg m^{-3}),

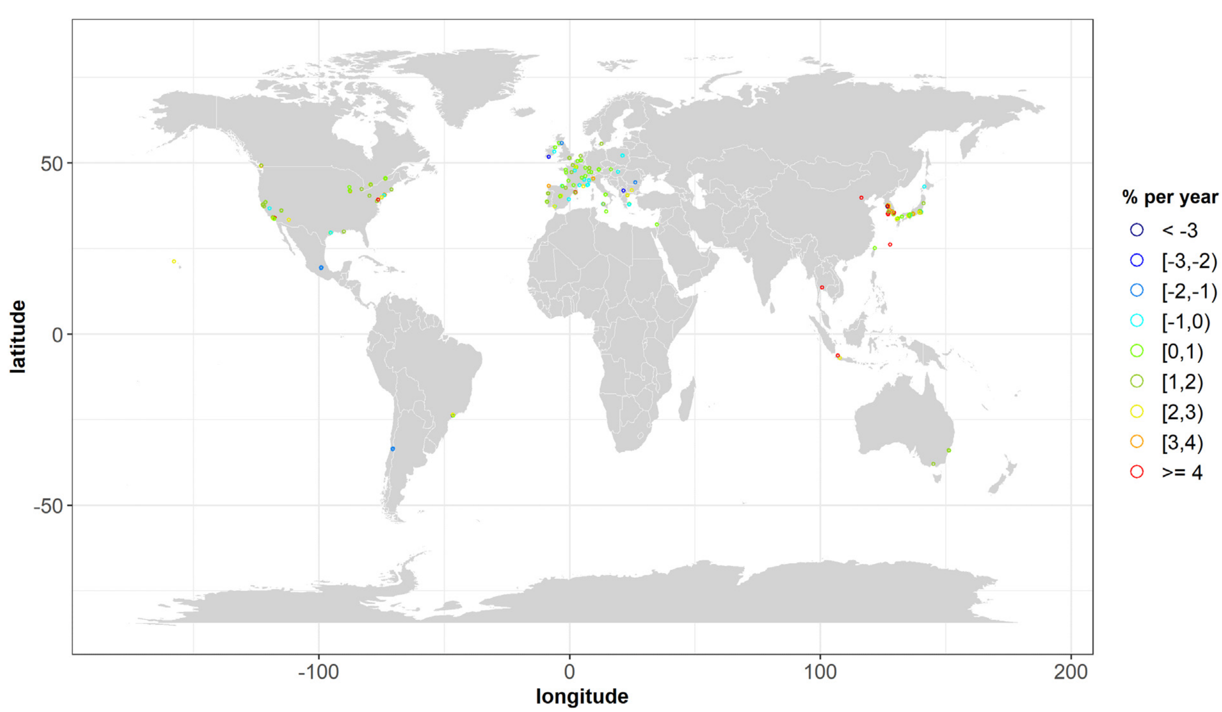

Fig. 5. Annual trends in annual O_3 mean concentration (in % per year) in urban areas with >50,000 inhabitants, from ground-based monitoring networks (Tropospheric Ozone Assessment Report), over the time period 2000–2019.

reflecting a wide variety of sources such as vehicular, industrial and biomass burning emissions (e.g., Singh et al., 2017; Zhang et al., 2018) while mineral dust sources were mostly dominant over North Africa and the Middle East (Weagle et al., 2018). Lower concentrations were reported over North America and Western Europe (<15 μg m^{-3}) reflecting regional emission controls (e.g., Simon et al., 2015; Li et al., 2017). The most polluted regions were South Asia, China, and India, and the less polluted regions were Europe and Japan (Zhang et al., 2020). Between 2000 and 2019, a large majority of the world's urban population (86 % in 2019, i.e., 2.5 billion people) lived in urban areas with $PM_{2.5}$ levels exceeding the WHO's 2005 limit value of 10 μg m^{-3} (Southerland et al., 2022). Most urban areas meeting the WHO AQG were in North and South America, Africa, and Europe (Southerland et al., 2022).

Apte et al. (2021) and Hammer et al. (2020) investigated satellite-derived surface $PM_{2.5}$ concentrations in 4231 urban areas (with >100,000 inhabitants) over the time period 1998–2018 and found similar results, i.e., about 2 % $year^{-1}$ reductions in $PM_{2.5}$ in the Eastern US and Western Europe, and 1–3 % $year^{-1}$ increases in $PM_{2.5}$ in South and Southeast Asia, the Middle East, South America and East Africa. The $PM_{2.5}$ levels decreased by 12 % in urban areas >50,000 inhabitants in Western Pacific (including China) and by 21 % in European urban areas between 2000 and 2019 (Southerland et al., 2022). In the EU-28, the annual $PM_{2.5}$ mean concentrations declined by 0.42 μg m^{-3} per year at 826 urban stations from 2000 to 2017 (European Environment Agency, 2019), in agreement with our result (0.32 μg m^{-3} $year^{-1}$) calculated from 706 urban areas in the EU-28 between 2000 and 2019.

Significant reductions in annual $PM_{2.5}$ mean concentrations were also reported in literature (Fig. 6, Table 7S) e.g., in Western Europe (Geddes et al., 2016; Khaniabadi and Sicard, 2021), at 390 urban sites in the US over the time period 2000–2020 (United States Environmental Protection Agency, 2021), and in the UK between 2005 and 2018 (Vohra et al., 2021). Similarly to our results, a substantial increase in $PM_{2.5}$ was reported in two large cities in India (Kanpur, and Delhi) in 2005–2018 (Vohra et al., 2021). The $PM_{2.5}$ mean concentrations increased in 350 Chinese prefectures during 1999–2011 (Han et al., 2015), while we reported a slight decrease between 2000 and 2019. In China, $PM_{2.5}$ emissions and concentrations continuously increased until 2007 as few air pollution control policies were implemented and driven by economic development (Xiao et al., 2020), and subsequently declined from 2013, with a 30–50 % decrease of annual mean $PM_{2.5}$ across China over 2013–2018 (Zhai et al., 2019).

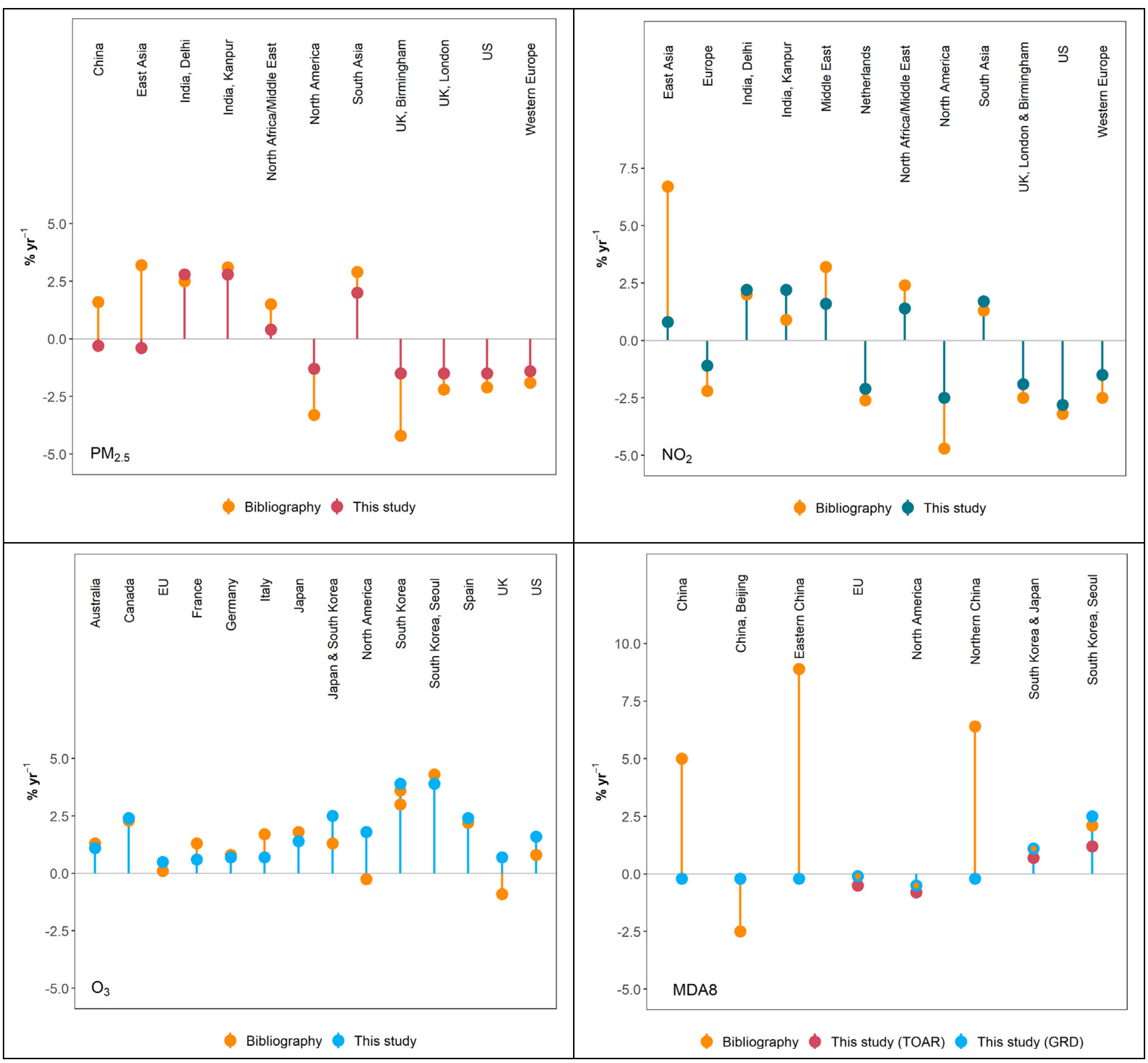

Fig. 6. Annual trends in annual $PM_{2.5}$, NO_2 and O_3 mean concentrations and of the highest seasonal average daily 8-h maximum O_3 concentration (in % $year^{-1}$) in urban areas, from literature (refers to Table 7S) compared to our study over the time period 2000–2019. For summertime O_3 MDA8, we also compared trends obtained in our study from ground-based monitoring networks (Tropospheric Ozone Assessment Report, TOAR) and the global reanalysis dataset (GRD) to literature.

Geddes et al. (2016) have estimated the trends in surface $PM_{2.5}$ from satellite-derived data over urban areas at 0.1° × 0.1° spatial resolution between 1998 and 2012, while we averaged the individual trends from the GRD by joining all urban centers e.g., in North America (388 urban centers) and East Asia (1926 urban centers).

4.2. Trends in NO_2 concentrations in urban areas

Higher annual NO_2 mean concentrations (>10 μg m^{-3}) were observed in Eastern US, Western Europe (Benelux) and Eastern China, reflecting a wide variety of sources such as transport, industry and/or coal-fired power stations, while lower concentrations (< 5 μg m^{-3}) were reported in Africa, Oceania, and Australia (Geddes et al., 2016; Achakulwisut et al., 2019). In 2019, <5 % of the EU-28 population was exposed to NO_2 concentrations above the WHO's 2005 AQG (40 μg m^{-3}), while this figure reaches 89 % by considering the recently updated version of WHO AQG (10 μg m^{-3}). About three-quarters of urban areas globally have NO_2 levels exceeding the new WHO AQG, i.e., about 77 % of the world's urban population (World Health Organization, 2022). Most urban areas meeting the WHO AQG are located in South Hemisphere and above 50°N latitude (Anenberg et al., 2022).

The estimated NO_2 concentration trends are consistent with previous studies in the US, Europe, Middle East, and Asia based on ground observations, satellite-derived data, and modeling outputs (e.g., Barkley et al., 2017; Georgoulias et al., 2019; Itahashi et al., 2019; Jamali et al., 2020; Qu et al., 2020; Zara et al., 2021). By applying a linear regression, Anenberg et al. (2022) found that the annual averaged NO_2 concentrations decreased globally by 13 % from 2000 to 2019 in 13,160 urban areas while the NO_2 levels increased by 18 % in South Asia and 11 % in sub-Saharan Africa (Anenberg et al., 2022). In the EU-28, the annual NO_2 mean concentrations declined by 0.39 μg m^{-3} per year by joining 708 urban stations between 2002 and 2011 (Guerreiro et al., 2014), and here we found a magnitude of 0.15 μg m^{-3} $year^{-1}$ by joining 720 urban areas between 2000 and 2019.

Similar trend magnitudes in surface NO_2 concentrations were reported in literature (Fig. 6, Table 7S) e.g., in Europe (Geddes et al., 2016), in the Netherlands (Zara et al., 2021), in the UK (Vohra et al., 2021), in North America (Geddes et al., 2016; Qu et al., 2020), in the Middle East (Geddes et al., 2016; Barkley et al., 2017), and in India (Vohra et al., 2021), and in South Asia (Geddes et al., 2016). Slight differences can be observed between our study and satellite-derived trends obtained by Geddes et al. (2016) in East Asia and North America over the time period 1996–2012. Tropospheric NO_2 decreased by 49 % over the US and the UK, by 36 % in Italy and Japan, and by 32 % over Germany and France; however, it was increased in developing regions, e.g., by 160 % in China and 33 % in India between 1996 and 2017 (Itahashi et al., 2019; Georgoulias et al., 2019).

4.3. Trends in urban population exposure to O_3

Higher surface O_3 levels were found in the North Hemisphere, highlighting a hemispheric asymmetry (Schultz et al., 2017). In urban areas, the highest annual O_3 mean concentrations (> 40 ppb) were observed around the Mediterranean basin (Sicard et al., 2013), in Western US, and in East Asia, while the lowest O_3 levels (< 15 ppb) were observed in South Hemisphere e.g., in Australia (Sicard et al., 2017). In the North Hemisphere, a latitudinal gradient was reported with lower O_3 concentrations in northern part ranging from 25 to 55 ppb (Schultz et al., 2017). The summer mean values of the O_3 MDA8 exceeded 60 ppb, with O_3 peaks frequently exceeding 120 ppb, in megacities in Southern Europe, Western US, and Eastern China, (e.g., Zhao and Wang, 2017; Li et al., 2018; Flynn et al., 2021). Almost the entire world's population (>90 %) lives in areas with air exceeding the O_3 safe level of the WHO's 2005 AQG (8 h daily max <50 ppb). In EU-28, over 95 % of the population was exposed to O_3 levels exceeding the WHO's 2005 AQG since 2000 (Sicard et al., 2021).

4.3.1. Trends in O_3 exposure

The simulated trends in summertime O_3 MDA8 calculated from the GRD are in full agreement with the trends obtained from ground-based measurements (TOAR database), and those reported in literature in Europe, North America, and East Asia between 2000 and 2019 (Fig. 6, Table 7S). For instance, by calculating the trends in summertime O_3 MDA8 from TOAR database, Chang et al. (2017) found a slight decrease at 260 urban stations in Europe (on average - 0.1 % $year^{-1}$) and at 140 urban stations in North America (on average - 0.5 % $year^{-1}$), while an increase was found in East Asia (on average + 1.1 % $year^{-1}$) in 2000–2014. In China, the simulated trends calculated from the GRD are much lower than those reported in literature (Liu et al., 2019; Xu et al., 2020; Yin et al., 2021; Bei et al., 2022) as the time period is shorter (from 2013 to 2019) and based on ground monitoring stations.

The trends in annual O_3 mean concentrations calculated from the GRD are in line with the trends obtained from ground-based monitoring networks, and those reported in literature (Fig. 6, Table 7S). Rising annual O_3 mean concentrations were previously reported for urban areas worldwide from the 1990s onward, in particular since 2005 (Sicard, 2021). The O_3 baseline level is rising in the urban areas in Australia, North America, Japan, and South Korea between 2000 and 2019 (Simon et al., 2015; Chang et al., 2017; Fleming et al., 2018; Jung et al., 2018; Kim and Lee, 2018; Yan et al., 2019; Sicard et al., 2020a). A slight difference is found in North America where Chang et al. (2017) reported a slight decrease at 140 urban stations (− 0.25 % $year^{-1}$) while an increase (+ 1.8 % $year^{-1}$) was found by joining 53 US urban centers (this study). Rising O_3 levels at urban stations were reported in Eastern China from 2001 onward (Gao et al., 2017; Sicard, 2021). For instance, the O_3 mean concentrations increased by 2.9 % $year^{-1}$ between 2007 and 2016 in Beijing (Xu et al., 2020). Africa (e.g., Ethiopia, Democratic Republic of the Congo, and Nigeria) and South Asia (e.g., India, Pakistan, and Bangladesh) were characterized by increased O_3 mean concentrations between 2010 and 2019. For example, Ethiopia and India experienced a steep increase of 27 % and 17 %, respectively (Health Effects Institute, 2020).

4.3.2. Trends in O_3 precursors emissions

In the US, on-road transport contributes to 41 % and 19 % of total NO_x and VOCs emissions, and the successive Tier standards have lowered the NO_x and VOCs emissions respectively by 55 % and 47 % between 2005 and 2018 (Sicard et al., 2020a). In European urban areas, the on-road transport emissions contribute to 8–10 % of ground level O_3 in winter and up to 15–24 % in summer (Mertens et al., 2019). In addition to vehicle emission regulations, the progress in the flue-gas treatments, in the storage and distribution of solvents, and the shift of power plants from coal to cleaner fuels e.g., natural gas (Lefohn et al., 2018; Zhang et al., 2018; Goldberg et al., 2019) led to NO_x and VOCs reductions e.g., in North America (NO_x: - 3.7 % $year^{-1}$; VOCs: - 3.3 % $year^{-1}$), in the EU-28 (NO_x: - 2.7 % $year^{-1}$; VOCs: - 2.6 % $year^{-1}$), and in East Asia (NO_x: + 4.3 % $year^{-1}$; VOCs: + 2.3 % $year^{-1}$) since 2000 (Zheng et al., 2018; Sicard et al., 2020a).

In spring and summer, the photochemistry plays a major role in the O_3 formation (Tørseth et al., 2012; Simon et al., 2015). The substantial reduction in O_3 precursor emissions led to a reduction in health-related metrics, e.g., summertime O_3 MDA8, and in O_3 peaks worldwide (de Foy et al., 2020; Akimoto and Tanimoto, 2022). However, in most urban areas under VOCs-limited regime, the O_3 mean concentrations increased due to a lowered titration of O_3 by NO (Bach et al., 2014; Huszar et al., 2015; Sicard et al., 2020a) following the implementation of stringent Directives to reduce local NO_x emissions e.g., in Canada (ECCC, 2016), Japan (Wang et al., 2014), South Korea (Seo et al., 2018), as well as across the EU (European Environment Agency, 2019) and the US (Simon et al., 2015; Winkler et al., 2018). High increases in O_3 mean concentrations, and summertime O_3 MDA8, were observed in South Korea in 2000–2019. The rising NO_x and VOCs emissions in China contribute up to 90 % to the O_3 MDA8 recorded in background stations in South Korea due to air mass transport (Kim and Lee, 2018). In China, the O_3 formation potential rose from

38.2 to 99.7 Tg of O_3 between 1990 and 2017 due to rising NO_x and VOCs emissions (Li et al., 2019).

To date, the national and European emissions control strategies focused more on NO_x than on VOCs and did not shift the chemical regimes from VOC- to NO_x-limited conditions, enhancing the O_3 formation in urban areas (Akimoto and Tanimoto, 2022). As effective long-term policy to reduce urban O_3 levels and human health risks, we recommend concurrent significant decrease of VOCs sources and slight changes in NO_x emissions (McDonald et al., 2018; Akimoto and Tanimoto, 2022). Green urban infrastructure can mitigate O_3 pollution in cities (Nowak et al., 2018). Biogenic VOCs (BVOCs) contribute up to 90 % of the total VOCs emissions, with 99 % of BVOCs emitted from vegetation (Cao et al., 2022). Hence, low VOCs emitting tree species should be selected for greening and re-naturing programs (Sicard et al., 2022).

To date, the spatial distribution of air quality monitoring stations is heterogeneous, in line with major population centers, e.g., Eastern US is well covered. Sparse spatial observations for air pollutants, particularly in Africa, do not provide a reliable source of data for the risk assessment of population to ambient air pollution. A fundamental question is whether the number and location of background monitoring stations are adequate to optimally cover a city. The spatial representativeness of urban background monitoring stations depends on e.g., air pollutants, location, urban spatial structure, population density, and dispersion dynamic of each pollutant. The median representative areas of urban background stations are 8–43 km^2 for NO_2, 35–79 km^2 for PM_{10}, and 94–105 km^2 for O_3, and drop to 0.5 km^2 and 0.6 km^2 for PM_{10} and NO_2, respectively for traffic stations (Kracht et al., 2017). More air quality monitors need to be installed in urban centers, but also in the countryside, to facilitate the risk assessment of rising air pollutants (e.g., O_3) and the generation of optimal maps as valuable tools for risk and exposure assessments.

5. Conclusions

The most $PM_{2.5}$-polluted (> 45 μg m^{-3}) regions in the world were the sub-Saharan Africa, and the East and South Asia, whereas the less polluted (< 15 μg m^{-3}) regions were Western Europe, the US, and Japan. Higher NO_2 concentrations (> 10 μg m^{-3}) were observed in Eastern US, Western Europe, and Eastern China, whereas lower concentrations (< 5 μg m^{-3}) occurred in the South Hemisphere, e.g., Oceania, and Australia. South Asia experienced the highest NO_2 exposures, which aligns with socioeconomic development and national policy actions. The highest O_3 exposures (> 40 ppb) were observed in the latitude band 15–45°N, particularly around the Mediterranean basin, while the lowest O_3 levels (< 15 ppb) were found in South Hemisphere.

Global exposure of urban population to $PM_{2.5}$ slightly declined from 2000 to 2019 (on av., − 0.2 % per year), and 65 % of the urban areas in the world showed an increase of annual $PM_{2.5}$ mean concentrations. From 2000 to 2019, some regions have experienced improvements, particularly Eastern US, Europe, Southeast China, and Japan. However, other regions have experienced increases in exposures, in particular the Middle East, sub-Saharan Africa, and Southeast Asia. The largest increases in annual $PM_{2.5}$ mean concentrations occurred in urban areas of South Asia (e.g., India, Bangladesh) between 2000 and 2019 while the largest improvement in $PM_{2.5}$ exposure occurred in Eastern China between 2000 and 2009 and 2010–2019.

At global scale, the annual NO_2 mean concentrations increased at 71 % of the urban areas between 2000 and 2019 (on av., + 0.4 % per year). From 2000 to 2019, some regions have experienced improvements, especially North America and Europe. The sub-Saharan Africa, Middle East, and South Asia regions have experienced increases in exposures. The population exposure to NO2 across these regions remained constant over the past two decades, with south Asia experiencing the highest exposures, in line with socioeconomic development and national policy actions (Anenberg et al., 2022). The largest improvements in NO_2 exposure occurred in Eastern China between both time periods 2000–2009 and 2010–2019.

On average, global exposure of urban population to O_3 increased between 2000 and 2019. The summertime O_3 MDA8 concentrations rose at 74 % of the urban areas worldwide (on av., + 0.6 % per year), while O_3 MDA8 showed a decline in North America, Northern Europe, and Southeast China, due to the substantial reduction in O_3 precursor emissions leading to reduced photochemical O_3 formation. The highest O_3 MDA8 increases (> 3 % per year) were reported in Equatorial Africa, South Korea, and India. However, the mean concentrations are sensitive to the NOx titration effect, and its concentrations increased in urban areas e.g., at 89 % of the 519 TOAR stations (on av. 0.8 % per year) between 2000 and 2019. The rising O_3 levels become a major public health issue in urban areas where the number of O_3-related premature deaths increased over time, e.g., + 0.55 deaths per 1,000,000 people in the EU-28 cities between 2000 and 2017 (Sicard et al., 2021). For health impact assessment, the metrics recommended by the WHO, e.g., O_3 MDA8 or SOMO35 (Sum of daily maximum of 8-h Ozone Means Over 35 ppb), summarize the highest exposure to O_3 over one year. Both O_3 MDA8 and SOMO35 do not account for rising background O_3 concentrations and their possible effects on human health over time. Hence, a need emerges to develop and use human health impact metrics with no concentration/exposure threshold, while also allowing the possibility of non-linear effects.

The establishment and implementation of emission control strategies, in individual countries worldwide, led to geographically heterogeneous magnitude of trends, in particular for surface O_3 levels, thus enlarging inequalities among countries and geographical regions. Cities influence their surroundings, but at the same time their air quality is heavily influenced by sources in the region of the city, other cities, or even other countries. For a cleaner air in cities, a cooperative approach across spatial scales and different level of governance is required, from city to conurbation, from local to regional. A stand-alone action by local authorities appeared to be insufficient to minimize air pollution-related health problems. There is an urgent need to take decisive actions at all governance levels to (i) reduce all the primary air pollutants simultaneously, ii) achieve the objectives of the recently updated WHO AQG, and (iii) reduce inequalities among countries (goal 10 of SDGs). Tackling global air pollution can help addressing several of the UN SDGs set forth to be achieved by 2030.

The huge literature about the COVID-19 lockdown effect on air pollution highlighted the challenge for reducing the formation of secondary pollutants (e.g., surface O_3) even with strict measures to control primary pollutant emissions (e.g., Sicard et al., 2020b; Tobías et al., 2020; Campbell et al., 2021; Miyazaki et al., 2021). As effective long-term abatement policies of urban pollution and human health risks in urban centers, we recommend significant reductions of PM and VOCs emissions concurrently with slight reductions in NO_x emissions, for instance with the regulation and enforcement of vehicle emission standards, the shift from coal to cleaner fuels (e.g., natural gas) in residential and industrial sectors (e.g., domestic heating), reduction in the emissions from biomass burning, livestock, heavy industries harboring iron and steel smelts, but also with stringent regulation of home and garden activities (e.g. cleaning, fireplaces, barbeques, green waste burning). For all air pollutants, the effectiveness and costs of reduction technologies should be considered (Tucker, 2000).

CRediT authorship contribution statement

P.S., and V.C. conceived the project. P.S., S.C.A., and V.C. gathered all data (data curation, collation). P.S., E.A., E.P. and A.D.M. analyzed data. P.S. wrote the original draft. All authors participated in writing, reviewing, and editing the manuscript.

Data availability

Data will be made available on request.

Declaration of competing interest

The authors declare that they have no known competing financial interests or personal relationships that could have appeared to influence the work reported in this paper.

Acknowledgements

This work was made in the framework of the Research Group 8.04.00 "*Air Pollution and Climate Change*" and under the Working Party 8.04.05 "Ground-level ozone" of the International Union of Forest Research Organizations (IUFRO). This work was carried out with the contribution of the LIFE financial instrument of the European Union in the framework of the AIRFRESH project "*Air pollution removal by urban forests for a better human well-being*" (LIFE19 ENV/FR/000086). V.C. thanks Project IMAGINA (PROMETEU 2019, Generalitat Valenciana). E.A. acknowledges support from the National Natural Science Foundation of China (No. 4210070867), the Startup Foundation for Introducing Talent (No. 003080) of NUIST, China, and the Jiangsu Distinguished Professor program of the People's Government of Jiangsu Province, China.

Appendix A. Supplementary data

Supplementary data to this article can be found online at https://doi.org/10.1016/j.scitotenv.2022.160064.

References

Achakulwisut, P., Brauer, M., Hystad, P., Anenberg, S.C., 2019. Global, national, and urban burdens of pediatric asthma incidence attributable to ambient NO2 pollution: estimates from global datasets. Lancet Planet. Health 3, e166–e178.

Agathokleous, E., Feng, Z., Oksanen, E., Sicard, P., Wang, Q., Saitanis, C.J., et al., 2020. Ozone affects plant, insect, and soil microbial communities: a threat to terrestrial ecosystems and biodiversity. Science Advances 6, eabc1176.

Akimoto, H., Tanimoto, H., 2022. Rethinking of the adverse effects of NOx-control on the reduction of methane and tropospheric ozone – challenges toward a denitrified society. Atmos. Environ. 277, 119033.

Anenberg, S., Miller, J., Minjares, R., Du, L., Henze, D.K., et al., 2017. Impacts and mitigation of excess diesel-related NOx emissions in 11 major vehicle markets. Nature 545, 467–471.

Anenberg, S.C., Mohegh, A., Goldberg, D.L., Kerr, G.H., Brauer, M., et al., 2022. Long-term trends in urban NO2 concentrations and associated paediatric asthma incidence: estimates from global datasets. Lancet Planet Health 6, e49–e58.

Apte, J., Seraj, S., Chambliss, S., Hammer, M., Southerland, V., Anenberg, S., et al., 2021. Air Inequality: Global Divergence in Urban Fine Particulate Matter Trends. 2021; published online ND Chem Rxiv https://doi.org/10.5281/zenodo.4777367 (preprint).

Araki, S., Yamamoto, K., Kondo, A., 2015. Application of regression kriging to air pollutant concentrations in Japan with high spatial resolution. Aerosol Air Qual. Res. 15, 234–241.

Bach, H., Brandt, J., Christensen, J.H., Ellermann, T., Geels, C., Hertel, O., Massling, A., Nielsen, H.Ø., et al., 2014. Services to Assess the Reasons for Non-compliance of Ozone Target Value Set by Directive 2008/50/EC and Potential for Air Quality Improvements in Relation to Ozone Pollution: Final Report. ECORYS, Rotterdam.

Barkley, M.P., González, Abad G., Kurosu, T.P., Spurr, R., Torbatian, S., Lerot, C., 2017. OMI air-quality monitoring over the middle east. Atmos. Chem. Phys. 17, 4687–4709.

Bei, N., Liang, J., Li, X., Wang, R., 2022. Worsening summertime ozone pollution in the Guanzhong Basin, China from 2014 to 2018: impacts of synoptic conditions and anthropogenic emissions. Atmos. Environ. 274, 118974.

Bell, M.L., Kim, J.Y., Dominici, F., 2007. Potential confounding of particulate matter on the short-term association between ozone and mortality in multisite time-series studies. Environ. Health Perspect. 115, 1591–1595.

Campbell, P.C., Tong, D., Tang, Y., Baker, B., Lee, P., Saylor, R., et al., 2021. Impacts of the COVID-19 economic slowdown on ozone pollution in the U.S. Atmos. Environ. 264, 118713.

Cao, J., Situ, S., Hao, Y., Xie, S., Li, L., 2022. Enhanced summertime ozone and SOA from biogenic volatile organic compound (BVOC) emissions due to vegetation biomass variability during 1981–2018 in China. Atmos. Chem. Phys. 22, 2351–2364.

Chang, K.L., Petropavlovskikh, I., Cooper, O.R., Schultz, M.G., Wang, T., 2017. Regional trend analysis of surface ozone observations from monitoring networks in eastern North America, Europe and East Asia. Elementa 5, 50.

Cohen, A.J., Brauer, M., Burnett, R., Anderson, H.R., Frostad, J., Estep, K., et al., 2017. Estimates and 25-year trends of the global burden of disease attributable to ambient air pollution: an analysis of data from the global burden of diseases study 2015. Lancet 389, 1907–1918.

ECCC, Environment and Climate Change Canada, 2016. Canada - United States Air Quality Agreement Progress Report 2016, p. 32 ISSN 1910-5223.

De Lang, M.N., Becker, J.S., Chang, K.L., Serre, M.L., Cooper, O.R., Schultz, M.G., et al., 2021. Mapping yearly fine resolution global surface ozone through the Bayesian maximum entropy data fusion of observations and model output for 1990–2017. Environ. Sci. Technol. 55, 4389–4398.

De Marco, A., Garcia-Gomez, H., Collalti, A., Khaniabadi, Y.O., Feng, Z., Proietti, C., Sicard, P., Vitale, M., Anav, A., Paoletti, E., 2022. Ozone modelling and mapping for risk assessment: an overview of different approaches for human and ecosystems health. Environ. Res. 211, 113048.

European Council Directive 2008/50/EC, 2008. European Council Directive 2008/50/EC of the European Parliament and of the Council of 21May 2008 on ambient air quality and cleaner air for Europe. Official Journal L 152, 0001–0044.

European Council Directive 2016/2284/EC, 2016. European Council Directive 2016/2284/EC of the European Parliament and of the Council of 14 December 2016 on the reduction of national emissions of certain atmospheric pollutants, amending Directive 2003/35/EC and repealing Directive 2001/81/EC. Official Journal of the European Union L 344 (1).

European Environment Agency, 2019. Air quality in Europe - 2019 report. EEA Technical Report No 10/2019. https://doi.org/10.2800/822355.

European Environment Agency, 2021. Air quality in Europe 2021. EEA Technical Report 15/2021. https://doi.org/10.2800/549289 ISBN 978-92-9480-403-7.

Fleming, Z.L., Doherty, R.M., von Schneidemesser, E., Malley, C.S., Cooper, O.R., Pinto, J.P., Colette, A., Xu, X., et al., 2018. Tropospheric ozone assessment report: present-day ozone distribution and trends relevant to human health. Elem. Sci. Anth. 6, 12.

Flynn, M.T., Mattson, E.J., Jaffe, D.A., Gratz, L.E., 2021. Spatial patterns in summertime surface ozone in the Southern Front Range of the U.S. Rocky Mountains. Elem Sci Anth 9, 1.

de Foy, B., Brune, W.H., Schauer, J.J., 2020. Changes in ozone photochemical regime in Fresno, California from 1994 to 2018 deduced from changes in the weekend effect. Environ. Pollut. 263, 114380.

Gao, W., Tie, X., Xu, J., Huang, R., Mao, X., Zhou, G., Chang, L., 2017. Long-term trend of O3 in a mega City (Shanghai), China: Characteristics, causes, and interactions with precursors. Sci Total Environ 603–604, 425–433.

Geddes, J.A., Martin, R.V., Boys, B.L., van Donkelaar, A., 2016. Long-term trends worldwide in ambient NO2 concentrations inferred from satellite observations for exposure assessment. Environ. Health Perspec. 124, 281–289.

Georgoulias, A.K., van der, A.R.J., Stammes, P., Boersma, K.F., Eskes, H.J., 2019. Trends and trend reversal detection in 2 decades of tropospheric NO2 satellite observations. Atmos Chem Phys. 19, 6269–6294.

Global Burden of Disease, 2019. Global burden of 369 diseases and injuries in 204 countries and territories, 1990–2019: a systematic analysis for the global burden of disease study 2019. Lancet 396 (2020), 1204–1222.

Goldberg, D.L., Lu, Z., Oda, T., et al., 2019. Exploiting OMI NO2 satellite observations to infer fossil-fuel CO2 emissions from U.S. megacities. Sci. Total Environ. 695, 133805.

Guerreiro, C.B.B., Foltescu, V., de Leeuw, F., 2014. Air quality status and trends in Europe. Atmos. Environ. 98, 376–384.

Hammer, M.S., van Donkelaar, A., Li, C., Lyapustin, A., Sayer, A.M., Hsu, N.C., et al., 2020. Global estimates and long-term trends of fine particulate matter concentrations (1998–2018). Environ. Sci. Technol. 54, 7879–7890.

Han, L., Zhou, W., Li, W., 2015. Increasing impact of urban fine particles (PM2.5) on areas surrounding Chinese cities. Sci. Rep. 5, 12467.

Health Effects Institute, 2020. State of Global Air 2020. Special ReportHealth Effects Institute, Boston, MA ISSN 2578-6873.

Hu, E., Ren, Z., Wang, X., Zhang, H., Zhang, W., 2022. Effect of elevated tropospheric ozone on soil carbon and nitrogen: a meta-analysis. Environ. Res. Lett. 17, 043001.

Huszar, P., Belda, M., Halenka, T., 2015. On the long-term impact of emissions from central European cities on regional air-quality. Atmos. Chem. Phys. Discuss. 15, 32101–32155.

Itahashi, S., Yumimoto, K., Kurokawa, J., Morino, Y., Nagashima, T., Miyazaki, K., Maki, T., Ohara, T., 2019. Inverse estimation of NOx emissions over China and India 2005–2016: contrasting recent trends and future perspectives. Environ. Res. Lett. 14, 124020.

Jamali, S., Klingmyr, D., Tagesson, T., 2020. Global-scale patterns and trends in tropospheric NO2 concentrations, 2005–2018. Remote Sens. 12, 3526.

Jerrett, M., Burnett, R.T., Pope, C.A., Ito, K., Thurston, G., et al., 2009. Long-term ozone exposure and mortality. New Engl. J. Med. 360, 1085–1895.

Jung, H.C., Moon, B.K., Wie, J., 2018. Seasonal changes in surface ozone over South Korea. Helyion 4, e00515.

Khaniabadi, Y.O., Sicard, P., 2021. A 10-year assessment of ambient fine particles and related health endpoints in a large Mediterranean city. Chemosphere 278, 130502.

Khomenko, S., Cirach, M., Pereira-Barboza, M.P.H., Mueller, N., Barrera-Gomez, J., Rojas-Rueda, D., de Hoogh, K., Hoek, G., Nieuwenhuijsen, M., 2021. Premature mortality due to air pollution in European cities: a health impact assessment. Lancet Planet. Health 5, e121–e134.

Kim, Y.P., Lee, G., 2018. Trend of air quality in Seoul: policy and science. Aerosol Air Qual. Res. 18, 2141–2156.

Kracht, O., Santiago, J.L., Martin, F., Piersanti, A., Cremona, G., Righini, G., et al., 2017. Spatial Representativeness of Air Quality Monitoring Sites - Outcomes of the FAIRMODE/AQUILA Intercomparison Exercise. Publications Office of the European Union, Luxembourg 2017, ISBN 978-92-79-77218-4, JRC108791.

Larkin, A., Geddes, J.A., Martin, R.V., et al., 2017. Global land use regression model for nitrogen dioxide air pollution. Environ. Sci. Technol. 51, 6957–6964.

Lefohn, A.S., Malley, C.S., Smith, L., Wells, B., Hazucha, M., Simon, H., et al., 2018. Tropospheric ozone assessment report: global ozone metrics for climate change, human health, and crop/ecosystem research. Elementa 6, 28.

Lelieveld, J., Evans, J.S., Fnais, M., Giannadaki, D., Pozzer, A., 2015. The contribution of outdoor air pollution sources to premature mortality on a global scale. Nature 525, 367–371.

Li, C., Martin, R.V., van Donkelaar, A., Boys, B.L., Hammer, M.S., Xu, J.W., Marais, E.A., Reff, A., Strum, M., Ridley, D.A., Crippa, M., Brauer, M., Zhang, Q., 2017. Trends in chemical composition of global and regional population-weighted fine particulate matter estimated for 25 years. Environ. Sci. Technol. 51, 11185.

Li, K., Jacob, D.J., Liao, H., Shen, L., Zhang, Q., Bates, K.H., 2018. Anthropogenic drivers of 2013–2017 trends in summer surface ozone in China. PNAS 116, 422–427.

Li, M., Zhang, Q., Zheng, B., Tong, D., Lei, Y., et al., 2019. Persistent growth of anthropogenic non-methane volatile organic compound (NMVOC) emissions in China during 1990–2017: drivers, speciation and ozone formation potential. Atmos. Chem. Phys. 19, 8897–8913.

Lin, M., Horowitz, L.W., Payton, R., Fiore, A.M., Tonnesen, G., 2017. US surface ozone trends and extremes from 1980 to 2014: quantifying the roles of rising Asian emissions, domestic controls, wildfires, and climate. Atmos. Chem. Phys. 17, 2943–2970.

Liu, F., Beirle, S., Zhang, Q., van der, A.R.J., Zheng, B., Tong, D., He, K., 2017. NOx emission trends over Chinese cities estimated from OMI observations during 2005 to 2015. Atmospheric Chem. Phys. 17, 9261–9275.

Liu, J., Wang, L., Li, M., Liao, Z., Sun, Y., Song, T., Gao, W., Wang, Y., Li, Y., Ji, D., Hu, B., Kerminen, V.M., Wang, Y., Kulmala, M., 2019. Quantifying the impact of synoptic circulation patterns on ozone variability in northern China from April to October 2013–2017. Atmos. Chem. Phys. 19, 14477–14492.

Lloyd, C.T., Chamberlain, H., Kerr, D., Yetman, G., Pistolesi, L., Stevens, F.R., et al., 2019. Global spatiotemporally harmonised datasets for producing high-resolution gridded population distribution datasets. Big Earth Data. 3, 108–139.

Malashock, D.A., Delang, M.N., Becker, J.S., Serre, M.L., West, J.J., et al., 2022. Estimates of Ozone Concentrations and Attributable Mortality 1 in Urban, Peri-Urban and Rural Areas Worldwide in 2019. ERL in press.

McDonald, B.C., de Gouw, J.A., Gilman, J.B., Jathar, S.H., Akherati, A., Cappa, C.D., et al., 2018. Volatile chemical products emerging as largest petrochemical source of urban organic emissions. Science 359 (6377), 760–764.

McDuffie, E., Martin, R., Yin, H., Brauer, M., 2021. Global Burden of Disease from Major Air Pollution Sources (GBD MAPS): A Global Approach. Research Report 210 Health Effects Institute, Boston, MA ISSN 2688-6855 (online).

MEP - Ministry of Environmental Protection, 2012. Government of China, Ambient Air Quality Standards (in Chinese) GB 3095-2012.

Mertens, M., Kerkweg, A., Grewe, V., Jöckel, P., Sausen, R., 2019. Attributing land transport emissions to ozone and ozone precursors in Europe and Germany. Atmos. Chem. Phys. Discuss. https://doi.org/10.5194/acp-2019-715.

Miyazaki, K., Bowman, K., Sekiya, T., Takigawa, M., Neu, J.L., Sudo, K., et al., 2021. Global tropospheric ozone responses to reduced NOx emissions linked to the COVID-19 worldwide lockdowns. ScienceAdvances 7, eabf7460.

Monks, P.S., Archibald, A.T., Colette, A., Cooper, O., Coyle, M., Derwent, R., Fowler, D., Granier, C., et al., 2015. Tropospheric ozone and its precursors from the urban to the global scale from air quality to short-lived climate forcer. Atmos. Chem. Phys. 15, 8889–8973.

Nowak, D.J., Hirabayashi, S., Doyle, M., McGovern, M., Pasher, J., 2018. Air pollution removal by urban forests in Canada and its effect on air quality and human health. Urban For. Urban Green. 29, 40–48.

Pascal, M., Corso, M., Chanel, O., Declercq, C., Badaloni, C., Cesaroni, G., et al., 2013. Assessing the public health impacts of urban air pollution in 25 European cities: results of the Aphekom project. Sci. Total Environ. 449, 390–400.

Perring, M.P., Bullock, J.M., Alison, J., Holder, A.J., Hayes, F., 2022. Out of sight, out of mind – but not out ofscope. The need to consider ozone in restoration science, policy, and practice. Restor. Ecol., e13622 https://doi.org/10.1111/rec.13622.

Qu, Z., Henze, D.K., Cooper, O.R., Neu, J.L., 2020. Improving NO2 and ozone simulations through global NOx emission inversions. Atmos. Chem. Phys. Discuss. 20, 13109–13130.

Schultz, M.G., Schröder, S., Lyapina, O., Cooper, O., Galbally, I., Petropavlovskikh, I., von Schneidemesser, E., Tanimoto, H., et al., 2017. Tropospheric ozone assessment report: database and metrics data of global surface ozone observations. Elem. Sci. Anth. 5, 58.

Seo, J., Park, D.S.R., Kim, J.Y., Youn, D., Lim, Y.B., Kim, Y., 2018. Effects of meteorology and emissions on urban air quality: a quantitative statistical approach to long-term records (1999–2016) in Seoul, South Korea. Atmos. Chem. Phys. 18, 16121–16137.

Shaddick, G., Thomas, M.L., Mudu, P., Ruggeri, G., Gumy, S., 2020. Half the world's population are exposed to increasing air pollution. Npj climate and atmospheric Science 3, 23.

Sicard, P., 2021. Ground-level ozone over time: an observation-based global overview. Curr. Opin. Environ. Sci. Health 19, 100226.

Sicard, P., De Marco, A., Troussier, F., Renou, C., Vas, N., Paoletti, E., 2013. Decrease in surface ozone concentrations at Mediterranean remote sites and increase in the cities. Atmos. Environ. 79, 705–715.

Sicard, P., Serra, R., Rossello, P., 2016. Spatio-temporal trends of surface ozone concentrations and metrics in France. Environ. Res. 149, 122–144.

Sicard, P., Anav, A., De Marco, A., Paoletti, E., 2017. Projected global ground-level ozone impacts on vegetation under different emission and climate scenarios. Atmos. Chem. Phys. 17, 12177–12196.

Sicard, P., Paoletti, E., Agathokleous, E., Araminienė, V., Proietti, C., et al., 2020a. Ozone weekend effect in cities: deep insights for urban air pollution control. Environ. Res. 191, 110193.

Sicard, P., De Marco, A., Agathokleous, E., Feng, Z., Xu, X., Paoletti, E., Diéguez Rodriguez, J.J., Calatayud, V., 2020b. Amplified ozone pollution in cities during the COVID-19 lockdown. Sci. Total Environ. 735, 139542.

Sicard, P., Agathokleous, E., De Marco, A., Paoletti, E., Calatayud, V., 2021. Urban population exposure to air pollution in Europe over the last decades. Environ. Sci. Eur. 33, 28.

Sicard, P., Agathokleous, E., De Marco, A., Paoletti, E., 2022. Ozone-reducing urban plants: choose carefully. Science 377 (6606), 585.

Simon, H., Reff, A., Wells, B., Xing, J., Frank, N., 2015. Ozone trends across the United States over a period of decreasing NOx and VOC emissions. Environ. Sci. Technol. 49, 186–195.

Singh, N., Murari, V., Kumar, M., Barman, S.C., Banerjee, T., 2017. Fine particulates over South Asia: review and meta-analysis of PM2.5 source apportionment through receptor model. Environ. Pollut. 223, 121–136.

Southerland, V.A., Brauer, M., Mohegh, A., Hammer, M.S., van Donkelaar, A., et al., 2022. Global urban temporal trends in fine particulate matter (PM2.5) and attributable health burdens: estimates from global datasets. Lancet Planet Health 6, e139–e146.

Tatem, A.J., 2017. WorldPop, open data for spatial demography. Sci. Data 31, 170004.

Tobías, A., Carnerero, C., Reche, C., Massagué, J., Via, M., Minguillón, M.C., et al., 2020. Changes in air quality during the lockdown in Barcelona (Spain) one month into the SARS-CoV-2 epidemic. Sci. Total Environ. 726, 138540.

Tørseth, K., Aas, W., Breivik, K., Fjæraa, A.M., Fiebig, M., et al., 2012. Introduction to the european monitoring and evaluation programme (EMEP) and observed atmospheric composition change during 1972–2009. Atmos. Chem. Phys. 12, 5447–5481.

Tucker, W.G., 2000. An overview of PM2.5 sources and control strategies. Fuel Process. Technol. 65–66, 379–392.

Turner, M.C., Jerrett, M., Pope, C.A., Krewski, D., Gapstur, S.M., et al., 2016. Long-term ozone exposure and mortality in a large prospective study. Am. J. Respir. Crit. Care Med. 193, 1134–1142.

United Nations, 2018. The World's Cities in 2016. Available onDepartment of Economic and Social Affairs. https://www.un.org.

United States Environmental Protection Agency, 2021. available on https://www.epa.gov/air-trends/particulate-matter-pm25-trends updated on 23 March 2021.

United States Federal Register, 2015. National Ambient Air Quality Standards for Ozone, 40 CFR Part 50, 51, 52, 53 and 58, pp. 65292–65468.

Vohra, K., Marais, E.A., Suckra, S., Kramer, L., Bloss, W.J., Sahu, R., Gaur, A., Tripathi, S.N., Van Damme, M., Clarisse, L., Coheur, P.F., 2021. Long-term trends in air quality in major cities in the UK and India: a view from space. Atmos. Chem. Phys. 21, 6275–6296.

Wang, Y.H., Hu, B., Ji, D.S., Liu, Z.R., Tang, G.Q., et al., 2014. Ozone weekend effects in the Beijing-Tianjin-Hebei metropolitan area, China. Atmos. Chem. Phys. 14, 2419–2429.

Weagle, C.L., Snider, G., Li, C., van Donkelaar, A., Philip, S., Bissonnette, P., Burke, J., Jackson, J., Latimer, R., Stone, E., et al., 2018. Global sources of fine particulate matter: interpretation of PM2.5 chemical composition observed by SPARTAN using a global chemical transport model. Environ. Sci. Technol. 52, 11670–11681.

Winkler, S.L., Anderson, J.E., Garza, L., Ruona, W.C., Vogt, R., Wallington, T.J., 2018. Vehicle criteria pollutant (PM, NOx, CO, HCs) emissions: how low should we go? Clim.Atmos. Sci. 1, 26.

World Health Organization, 2022. Billions of people still breathe unhealthy air: new WHO data. Available online https://www.who.int (4 April 2022).

Xiao, Q., Geng, G., Liang, F., Wang, X., Lv, Z., Lei, Y., Huang, X., Zhang, Q., Liu, Y., He, K., 2020. Changes in spatial patterns of PM2.5 pollution in China 2000–2018: impact of clean air policies. Environ. Int. 141, 105776.

Xu, X., Lin, W., Xu, W., Jin, J., Wang, Y., et al., 2020. Long-term changes of regional ozone in China: implications for human health and ecosystem impacts. Elementa 8, 13.

Yan, Y., Lin, J., Pozzer, A., Kong, S., Lelieveld, J., 2019. Trend reversal from high-to-low and from rural-to-urban ozone concentrations over Europe. Atmos. Environ. 213, 25–36.

Yin, H., Lu, X., Sun, Y., Li, K., Gao, M., Zheng, B., Liu, C., 2021. Unprecedented decline in summertime surface ozone over eastern China in 2020 comparably attributable to anthropogenic emission reductions and meteorology. Environ. Res. Lett. 16, 124069.

Zara, M., Boersma, K.F., Eskes, H., Denier van der Gon, H., Vilà-Guerau de Arellano, J., Krol, M., van der Swaluw, E., Schuch, W., Velders, G.J.M., 2021. Reductions in nitrogen oxides over the Netherlands between 2005 and 2018 observed from space and on the ground: decreasing emissions and increasing O3 indicate changing NOx chemistry. Atmos. Environ. 9, 100104.

Zhai, S., Jacob, D.J., Wang, X., Shen, L., Li, K., Zhang, Y., Gui, K., Zhao, T., Liao, H., 2019. Fine particulate matter (PM2.5) trends in China, 2013–2018: separating contributions from anthropogenic emissions and meteorology. Atmos. Chem. Phys. 19, 11031–11041.

Zhang, R., Wang, Y., Smeltzer, C., Qu, H., Koshak, W., Boersma, K.F., 2018. Comparing OMI-based and EPA AQS in situ NO2 trends: towards understanding surface NOx emission changes. Atmos. Meas. Tech. 11, 3955–3967.

Zhang, L., Wilson, J.P., MacDonald, B., Zhang, W., Yu, T., 2020. The changing PM2.5 dynamics of global megacities based on long-term remotely sensed observations. Environ. Int. 142, 105862.

Zhao, Z., Wang, Y., 2017. Influence of the West Pacific subtropical high on surface ozone daily variability in summertime over eastern China. Atmos. Environ. 170, 197–204.

Zheng, B., Tong, D., Li, M., Liu, F., Hong, C., Geng, G., Li, H., Li, X., Peng, L., Qi, J., Yan, L., Zhang, Y., Zhao, H., Zheng, Y., He, K., Zhang, Q., 2018. Trends in China's anthropogenic emissions since 2010 as the consequence of clean air actions. Atmos. Chem. Phys. 18, 14095–14111.